ACS OMEGA

http://pubs.acs.org/journal/acsodf

Article

Thiocarbohydrazone and Chalcone-Derived 3,4-Dihydropyrimidinethione as Lipid Peroxidation and Soybean Lipoxygenase Inhibitors

Nikitas Georgiou, Eleni Chontzopoulou, Antigoni Cheilari, Aikaterini Katsogiannou, Danai Karta, Kyriaki Vavougyiou, Dimitra Hadjipavlou-Litina, Uroš Javornik, Janez Plavec, Demeter Tzeli,* Stamatia Vassiliou,* and Thomas Mavromoustakos*

Cite This: *ACS Omega* 2023, 8, 11966−11977

Read Online

ACCESS | Metrics & More | Article Recommendations | Supporting Information

ABSTRACT: The potential of the 4,6-diphenyl-3,4-dihydropyrimidine-2(1*H*)-thione (abbreviated as **KKII5**) and (*E*)-*N*′-benzylidenehydrazinecarbothiohydrazide (abbreviated as **DKI5**) compounds as possible drug leads is investigated. **KKII5** and **DKI5** are synthesized in high yield of up to 97%. Their structure, binding in the active site of the LOX-1 enzyme, and their toxicity are studied via joint experimental and computational methodologies. Specifically, the structure assignment and conformational analysis were achieved by applying homonuclear and heteronuclear 2D nuclear magnetic resonance (NMR) spectroscopy (2D-COSY, 2D-NOESY, 2D-HSQC, and 2D-HMBC) and density functional theory (DFT). The obtained DFT lowest energy conformers were in agreement with the NOE correlations observed in the 2D-NOESY spectra. Additionally, docking and molecular dynamics simulations were performed to discover their ability to bind and remain stabile in the active site of the LOX-1 enzyme. These in silico experiments and DFT calculations indicated favorable binding for the enzyme under study. The strongest binding energy, −9.60 kcal/mol, was observed for dihydropyrimidinethione **KKII5** in the active site of LOX-1. ADMET calculations showed that the two molecules lack major toxicities and could serve as possible drug leads. The redox potential of the active center of LOX-1 with the binding molecules was calculated via DFT methodology. The results showed a significantly smaller energy attachment of 2.8 eV with **KKII5** binding in comparison to **DKI5**. Thus, **KKII5** enhanced the ability of the active center to receive electrons compared to **DKI5**. This is related to the stronger binding interaction of **KKII5** relative to that of **DK15** to LOX-1. The two very potent LOX-1 inhibitors exerted IC_{50} 19 μM (**KKII5**) and 22.5 μM (**DKI5**). Furthermore, they both strongly inhibit lipid peroxidation, namely, 98% for **KKII5** and 94% for **DKI5**.

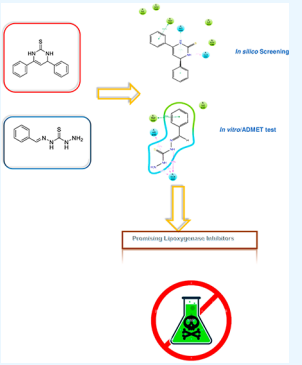

INTRODUCTION

Chalcones,[1,2] in particular, flavonoids, are natural products that display a broad spectrum of activities such as anticancer,[3] antibacterial,[4] antifungal,[5] antimalarial,[6] antidiabetic,[7] anti-inflammatory,[8] lipoxygenase inhibition,[9,10] and antioxidant.[11] Representatives of this class of compounds are already used in clinical practice or are undergoing clinical trials, including metochalcone,[12] sofalcone,[13] isoliquiritigenin,[14] xanthohumol,[15] hesperidin, and methylchalcone.[16,17]

Thiocarbohydrazones are an important, though less studied, class of molecules possessing biochemical, pharmaceutical, and industrial applications.[18] Of utmost importance is their metal-chelating ability.[19]

3,4-Dihydropyrimidines are important intermediates in the synthesis of bioactive molecules like natural products,[20] functional materials like polymers,[21] and adhesives.[22] In particular, 4,6-diaryl-3,4-dihydropyrimidine-2(1*H*)-thione derivatives were recently proven to possess potent cytotoxic activity.[23−25]

Combining anti-inflammatory activity with antioxidant capacity[26,27] in one drug turns out to be important for some therapies, including for COVID-19.[28] Toward this end, in the present study, thiocarbohydrazone **DKI5** and chalcone-derived 3,4-dihydropyrimidinethione **KKII5** were rationally designed through molecular docking and dynamics in silico and toxicity predictions, synthesized and evaluated for their antioxidant capacity as well as anti-inflammatory[29] agents through their ability to inhibit soybean lipoxygenase.

Lipoxygenases (LOXs) constitute an important iron-containing enzyme family. They catalyze hydroperoxidation of polyunsaturated fatty acid derivatives, containing a *cis,cis*-1,4-pentadiene moiety (e.g., arachidonic and linoleic

Received: November 29, 2022
Accepted: March 2, 2023
Published: March 21, 2023

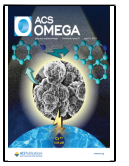

Scheme 1. Overall Diagram of This Research Work

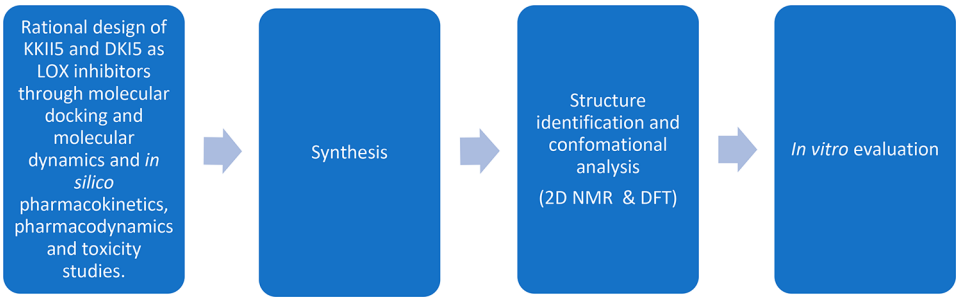

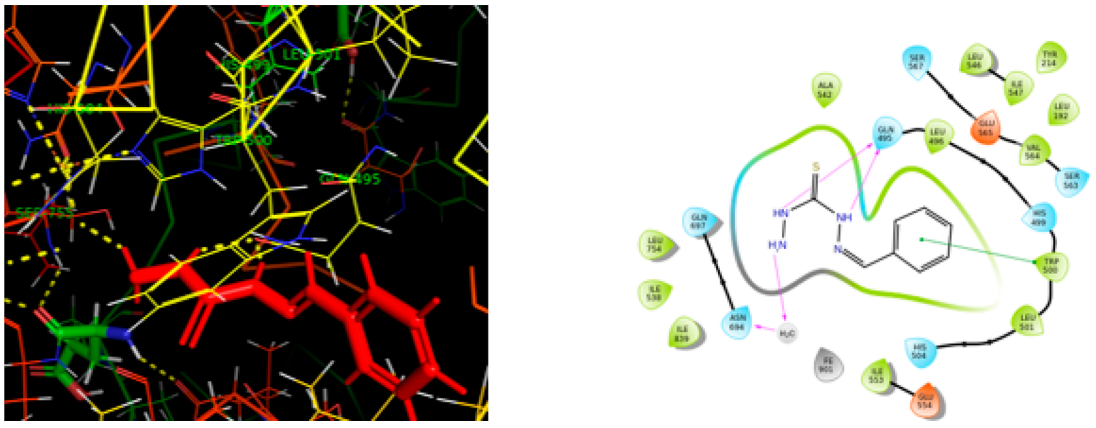

Figure 1. Interactions of **DKI5** with LOX-1 in 3D (left) and 2D (right) docking poses.

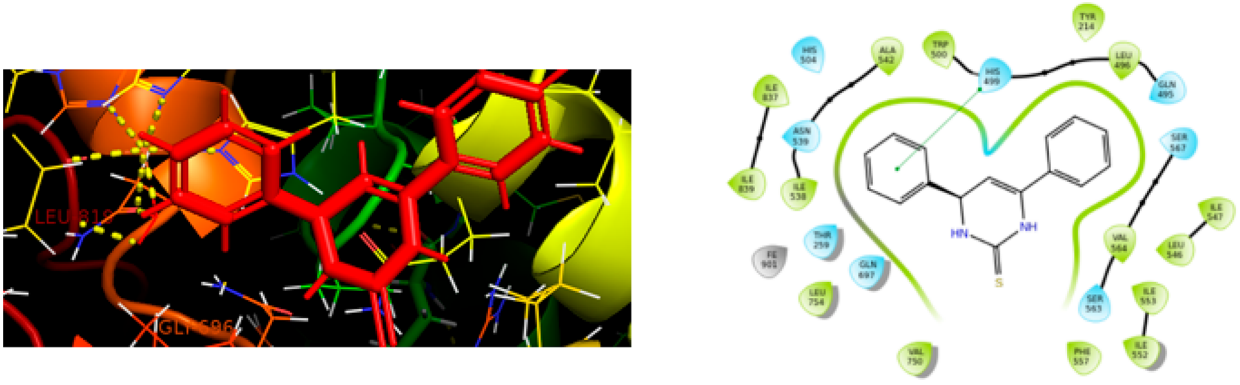

Figure 2. Interactions of **KKII5** with LOX-1 in 3D (left) and 2D (right) docking poses.

acids).[30,31] Their role in many acute and chronic diseases such as inflammation, cancer, asthma, allergy, and stroke has been well established.[32] Due to their potential as therapeutic targets, there is great interest for the discovery and synthesis of novel and potent LOX inhibitors. LOX inhibitors exert their mechanism of action as (i) redox inhibitors or antioxidants by interfering with the redox cycle of hydroperoxidation, (ii) iron chelator agents that directly form a complex with iron core of the enzyme, and (iii) nonredox competitive inhibitors.[33] Most of the redox inhibitors exert their action by using their radical scavenging property.

The rational design was achieved through molecular docking, molecular dynamics, density functional theory (DFT) and in silico pharmacokinetics, pharmacodynamics, and toxicity studies. Their promising profile led to the synthesis and structure identification of their conformational properties. Finally, their in vitro activity was evaluated. This strategy led to the identification of two of the most potent soybean LOX-1 and lipid peroxidation inhibitors. To the best of our knowledge, this is the first study leading to a thiocarbohydrazone and a 3,4-dihydropyrimidinethione as LOX-1 and lipid peroxidation inhibitors. The steps described above are illustrated in Scheme 1.

RESULTS AND DISCUSSION

Molecular Binding to the Active Site of Soybean LOX-1. Induced fit docking was utilized to study the possible binding mode of the two compounds in the active site of LOX-1. **DKI5** binds strongly to the active site of LOX-1. The ΔG_{bind} value has been calculated to be −7.14 kcal/mol. The molecule forms three hydrogen bonds with the residues of the cavity, which contributes to the strength of the binding. In particular, two H-bonds are formed between the hydrogen atoms of the thiourea functional group with GLN495, and one H-bond is

https://doi.org/10.1021/acsomega.2c07625
ACS Omega 2023, 8, 11966−11977

observed with one of the hydrogen atoms of the amine functional group and the water molecule in the first coordination sphere of an Fe cation. In addition, a $\pi-\pi$ stacking interaction is observed between the aromatic ring of the molecule and indole group of TRP500 (Figure 1).

In addition, **KKII5** binds strongly to the active site of LOX-1 indicating ΔG value of −9.60 kcal/mol. **KKII5** interacts with HIS499 of the cavity by forming one $\pi-\pi$ stacking interaction between the phenyl ring of the molecule and the imidazole ring of HIS499. Furthermore, two aromatic hydrogen bonds are formed between H9 and H12 (see Figure 2) with the residues GLN495 and ILE839, respectively.

Molecular Dynamics. Molecular dynamics simulations have been applied to assess the stability of the formed complexes and predict a more accurate conformation that the two aforementioned molecules adopt inside the active site of LOX-1. The docking poses described above (docking poses) have been used as the initial systems for the MD simulations.

As described in the diagram above, both enzyme−inhibitor simulations have been converged, since it is observed that, after the first 30 ns, the RMSD (root mean square deviation) of the protein does not present any significant changes until the completion of the simulation. In particular, the protein in the "enzyme−**KKII5**" complex has been stabilized at ∼2.11 Å, while the "enzyme−**DKI5**" complex has been stabilized at ∼1.97 Å (Figure 3).

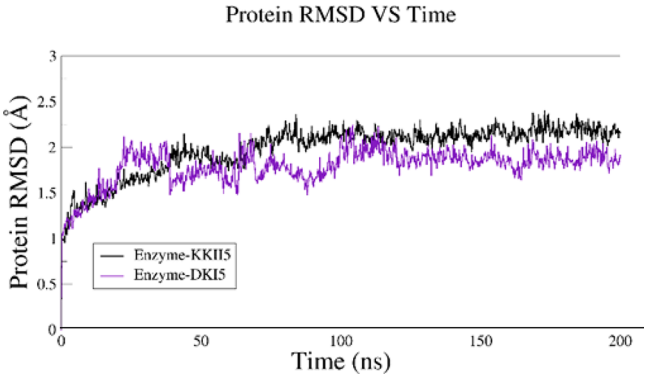

Figure 3. RMSD of the protein for the "enzyme−**KKII5**" complex (black line) and for the "enzyme−**DKI5**" complex (purple line) throughout the whole simulation (200 ns). The RMSD value was calculated based on the initial docking pose (first snapshot of the MD), which is used as a reference snapshot.

Molecular Dynamics Simulations of the "Enzyme−KKII5" Complex. According to the MD studies, **KKII5** remains bound to the active site of the enzyme during the production time. The conformations that the inhibitor adopts inside the cavity do not present significant changes in comparison to the initial docking pose (reference pose), and the orientation of the molecule remains similar to the first MD snapshot. In particular, the first phenyl ring is oriented toward HIS499, while the second is toward TRP500. Moreover, the key interactions that are formed between the molecule and the residues of the cavity were preserved from the docking studies throughout the whole simulation. The $\pi-\pi$ stacking interaction that was formed between the aromatic ring and the imidazole group of HIS499 in the first coordination sphere of iron was preserved for 31% of the simulation time, while the same type of interaction observed between the second phenyl ring and the indole group of TRP500 was for 55% of the simulation time. Furthermore, one hydrogen bond between the hydrogen atom of the thiopyrimidine ring and the oxygen atom of LEU546 was also preserved for 19% of the simulation time and another H-bond between the second hydrogen of thiopyrimidine ring and the oxygen atom of GLN495 (36% of the simulation time) (Figure 4).

To depict these results and present a more accurate pose of the ligand inside the LOX's cavity, a trajectory cluster analysis was performed based on ligands' conformations in the active site. Hence, the conformation that governed during the simulation in terms of time lasted for 49% of the simulation time. This statistically predominant conformation is illustrated in the figure below, and the RMSD calculated between the pose that derived from cluster analysis in comparison to the pose derived by docking calculations is equal to 1.79 Å (Figure 5).

Molecular Dynamics Simulations of the "Enzyme−DKI5" Complex. The inhibitor remains bound to the active site of the enzyme during the whole simulation time. The conformations that the inhibitor adopts inside the cavity do not change significantly in comparison to the initial docking pose regarding the orientation of the molecule, and the phenyl ring is oriented toward TRP500, while the diazole group is oriented toward the residues in the iron's first coordination sphere. Moreover, the key interactions that were observed during the docking studies between the molecule and the residues of the cavity were preserved in the MD simulation. The only minor change that was observed is that the whole molecule was slightly displaced away from the iron in the pose derived by the MD studies. The amine group is now in vicinal proximity with HIS499, in comparison to its proximity to the water molecule from the docking pose. In particular, the observed $\pi-\pi$ stacking interaction between the phenyl ring and the indole group of TRP500 was present for 85% of the simulation time. Furthermore, two hydrogen bonds between the hydrogens of the thiopyrimidine ring and the oxygen atom of GLN495 were present for 97 and 54% of the simulation time, respectively. In addition, the amine group of the molecule forms one H-bond with GLN495 (51% of the simulation time). Finally, an additional hydrogen bond between the hydrogen of the pyrimidine group and HIS499 is observed (Figure 6).

We performed trajectory cluster analysis based on the ligands' conformations to depict these results and present a more accurate pose of the ligand inside the LOX's cavity after the MD studies. In particular, the conformation that governed the simulation in terms of time lasted for 32% of the whole simulation time. This statistically predominant conformation is illustrated in the figure below, and the RMSD calculated between the pose that was derived from cluster analysis in comparison to the pose derived by docking calculations is equal to 0.009 Å (Figure 7).

MM/GBSA Calculations. MM/GBSA calculations were performed to the most favored energetic complexes extracted from Desmond trajectory clustering. MM/GBSA calculations are considered to be an adequate method to rank compounds targeting the same enzyme and to discover the key interactions that govern the binding of the compounds to the active site. In the table below, the binding energies of the two molecules under study are illustrated. According to the ΔG_{bind} values shown in the table, both compounds bind strongly to the active site of soybean LOX-1, which complements the results that have been already obtained by docking and MD simulations. In

https://doi.org/10.1021/acsomega.2c07625
ACS Omega 2023, 8, 11966−11977

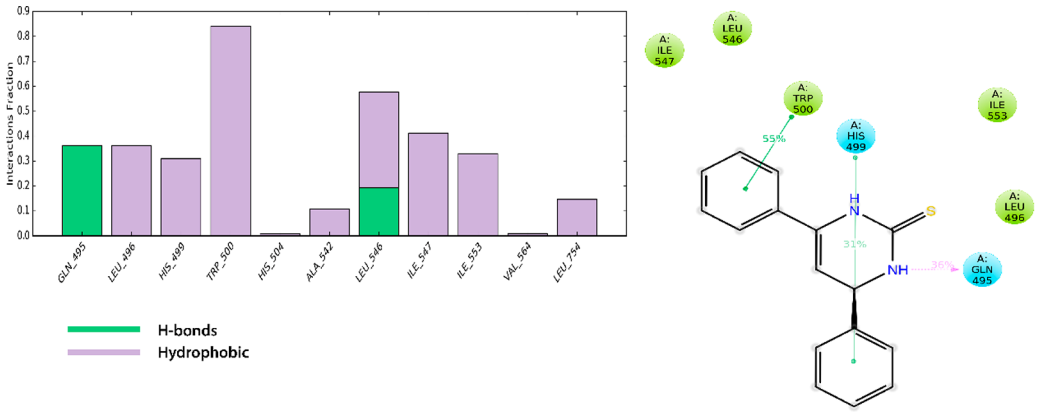

Figure 4. (Left) Protein–ligand interaction fraction shown by bars. The values are normalized over the trajectory period of 200 ns. (Right) Protein–ligand interactions. H-bonds are illustrated with purple dotted lines and π–π interactions with a solid green line.

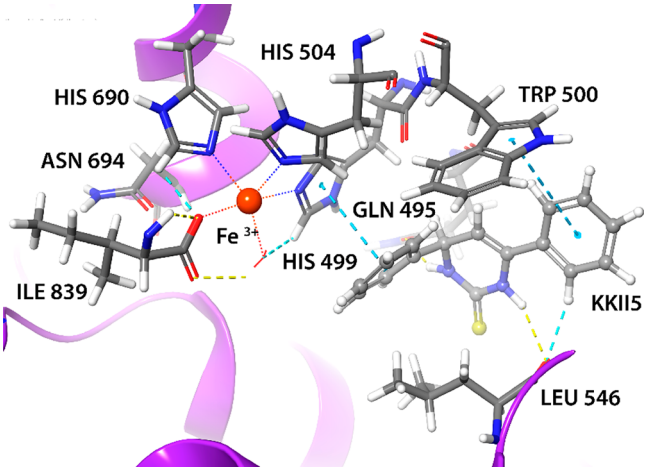

Figure 5. Three-dimensional pose of the active site of the "LOX–**KKII5**" complex derived after trajectory cluster analysis based on the ligands' conformations. This pose was adopted for 49% of the simulation time (200 ns).

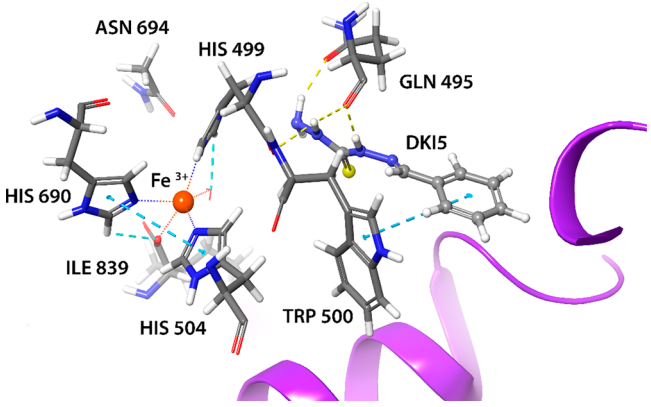

Figure 7. Three-dimensional pose of the active site of the "LOX–**DKI5**" complex derived after trajectory cluster analysis based on ligands' conformations. This pose was adopted for 32% of the simulation time (200 ns).

particular, for the most prominent cluster of the "LOX-1–**KKII5**" complex (49% of the simulation time), ΔG_{bind} is calculated to be −39.58 kcal/mol, while the most prominent cluster of the "LOX-1–**DKI5**" complex (32% of the simulation time), the ΔG_{bind} value is a little lower (−37.81 kcal/mol). Hence, we could conclude that the inhibitors present binding with similar strength to the active site of LOX-1, and thus we

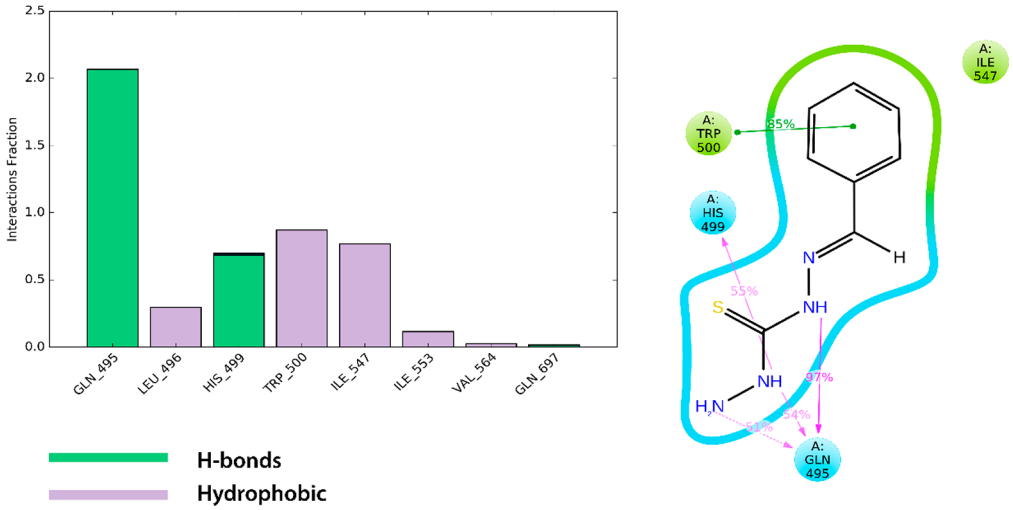

Figure 6. (Left) Protein–ligand interaction fraction shown by bars. The values are normalized over the trajectory period of 200 ns. (Right) Protein–ligand interactions. H-bonds are illustrated with purple dotted lines and π–π interactions with a solid green line.

https://doi.org/10.1021/acsomega.2c07625
ACS Omega 2023, 8, 11966–11977

Table 1. ΔG_{bind} Values Derived from MM/GBSA Calculations Based on the Statistically Predominant Cluster of MD Simulations

	ΔG_{bind} (kcal/mol)	ΔG_{bind} Coulomb	ΔG_{bind} H-bond	ΔG_{bind} Lipo	ΔG_{bind} packing	ΔG_{bind} Solv GB	ΔG_{bind} vdW
KKII5	−39.58	−9.31	−0.62	−28.76	−3.13	54.54	−52.31
DKI5	−37.81	−17.21	−1.11	−16.28	−1.13	35.36	−37.46

expect they will also illustrate similar IC_{50} values in the in vitro experiments as it is observed.

In order to further analyze the binding and discover the key factors that govern the "enzyme−ligand" complexation, we performed an energy decomposition analysis to the predominant cluster derived from MD simulations for both compounds.

Although the two compounds have similar ΔG_{bind} values, they show considerable different interactions. **DK15** shows increased Coulomb interactions presumably due to the additional amino group in its structure. **KK15** is apparently more lipophilic (log*P* = 3.01 average of the five values using SwissADME) than **DK15** (log*P* = 1.12 average of the five values using SwissADME) and shows stronger lipophilic and van der Waals interactions.

ADMET Calculations. The possible toxicity was predicted for both molecules under study by using SwissADME,[34] pkCSm,[35] and preADMET[36] computational tools (platforms). The compounds were predicted as nontoxic, and their structural properties reveal that they could serve as prominent drugs. For that reason, we proceeded to further analyze both (Tables 1S, 2S, and 3S).

Synthesis. The synthesis of studied compounds is illustrated in Schemes 1 and 2. Benzaldehyde reacted with thiocarbohydrazide in warm ethanol to give thiocarbohydrazone derivative **DKI5** (Scheme 2).

Scheme 2. DKI5 Synthesis

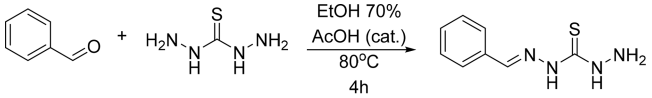

3,4-Dihydropyrimidine **KKII5** was prepared by cyclocondensation of chalcone **KKI1** (obtained from the reaction of benzaldehyde with acetophenone) with thiourea in the presence of NaOH with ultrasonication at room temperature (Scheme 3).

Structure Assignment. Scheme 4 shows the two compounds under study. The numbering will be used for the NMR structural assignment.

The structure assignment of **DK15** was initiated using the readily assigned H-6, which resonates at 8.01 ppm. Its signal gives integration of two protons, and it was the most shielded protons. Through 2D HSQC (Figure S3A), the H-6 shows $^{1}J_{C-H}$ coupling with the C6, and therefore, C6 is assigned

Scheme 4. Structures of (Left) DKI5 and (Right) KKII5 Compounds

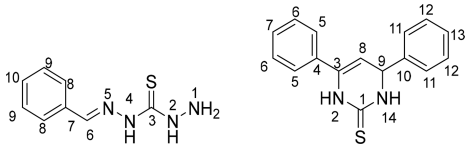

unambiguously at 143 ppm. H-8 is identified easily through 2D-NOESY (Figure S1A) due to its spatial proximity with H-6. Through 2D-NOESY, H-9 and H-10 are identified at 7.40 and 7.42 ppm. Protons attached with nitrogen are identified at 4.88, 9.82, and 11.43 ppm. Through a two-dimensional heteronuclear single quantum coherence (HSQC) spectrum of **KKI15**, all of the carbons bearing protons were identified. The quaternary and carbonyl carbons were identified through 2D-heteronuclear multiple bond coherence (HMBC) (Figure S4A). Specifically, H-9 shows a $^{3}J_{C-H}$ coupling with C-7, and H-2 shows a $^{2}J_{C-H}$ coupling with C-3.

The experimental data were carried out in DMSO solvent as it simulates the amphoteric environment and is suitable for the observation of NOE effects.[37,38] The same procedure was performed for **KKII5**.

Using $^{1}H-^{15}N$ (HSQC) and (HMBC)[39] experiments, we identified all of the nitrogen atoms on both molecules (Figures S1C, S2C and S3C).

The identification strategy is shown in the Supporting Information (Figures S1D and S2D). Proton spectra of **KKII5** and **DKI5** are shown below (Figure 8). Furthermore, Table 2 with the chemical shifts of these compounds is shown below.

DFT Conformational Analysis of DKI5 and KKII5. The lowest in energy structures of **DKI5** (a) and **KKII5** (b) are shown below. As these are in harmony with 2D-NOESY spectra, thye are considered as the most probable conformations for **KKII5** and **DKI5** (see Figure 9).

The characterization of the compounds by ^{1}H NMR and ^{13}C NMR indicates one predominant isomeric form in DMSO for each compound. The planes of phenyl groups B *και* C in **KKII5** are perpendicular to each other, and A and B are coplanar to each other, having the potential to form a better interaction with the active center of LOX-1.

The spatial correlations that are observed in 2D-NOEs are shown in Figure 10.

Redox Potential. The binding of **DKI5** and **KKII5** in the active site of LOX-1 (see Figures 5 and 7) was calculated via DFT (B3LYP/6-311+G(d,p)) methodology. The redox

Scheme 3. KKII5 Synthesis

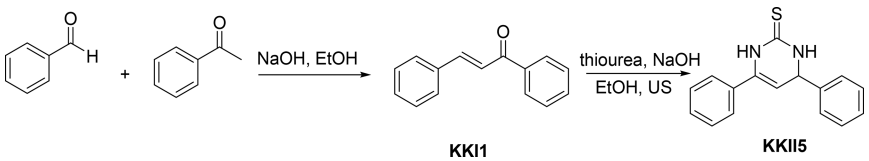

https://doi.org/10.1021/acsomega.2c07625
ACS Omega 2023, 8, 11966−11977

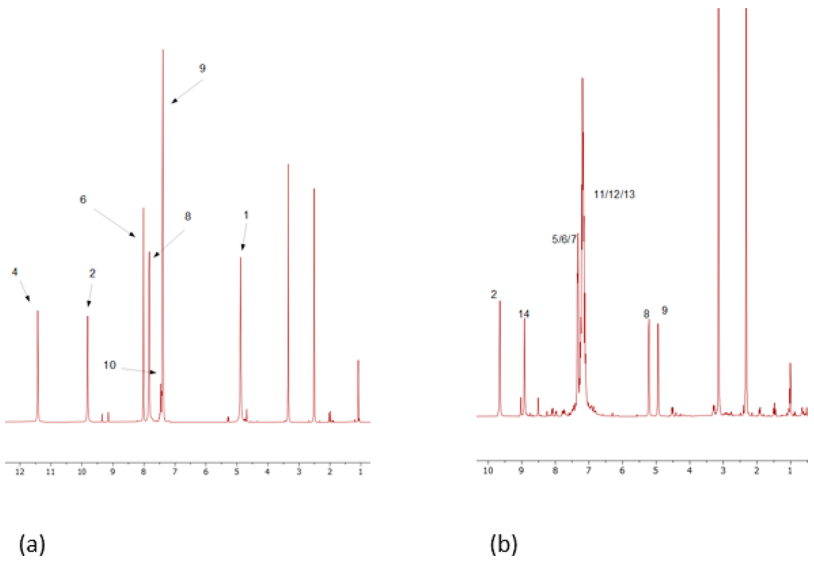

Figure 8. ^{1}H NMR spectra in DMSO-d_6 of **DKI5** (a) and **KKII5** (b). The spectra were recorded on a Bruker AC 400 MHz spectrometer at 25 °C.

Table 2. Assignment of the Experimental ^{1}H NMR Spectra of DKI5 (Top) and KKII5 (Bottom) in DMSO-d_6

position (**DKI5**)	^{1}H	NOESY	HSQC	HMBC	^{13}C
1	4.88	H-2/H-4/H-6/H-8/H-9/H-10			
2	9.82	H-1/H-4		C-3	
3				H-2/H-4	176.11
4	11.43	H-1/H-2/H-6		C-3/C-6	
5					
6	8.015	H-1	C-6	H-4/H-8/C-7/C-8/C-9	143
7				H-6/H-8/H-9	135
8	7.83		C-8	H-6/H-9/H-10/C-6/C-7/C-9/C-10	127.85
9	7.4		C-9	H-6/H-8/H-9/H-10/C-7/C-8/C-9/C-10	128.9
10			C-10	H-8/H-9/C-8/C-9	130

position (**KKII5**)	^{1}H	NOESY	HSQC	HMBC	^{13}C
1				H-14/H-2	175.63
2	9.65	H-4		C-1/C-3	
3				H-2	134.82
4				H-5/H-6	133.79
5	7.32	H-8	C-5	C-4/C-6	128.50
6	7.32	H-5/H-4	C-6	H-7/H-5	128.50
7	7.32	H-6	C-7	H-6/H-5	128.50
8	5.22	H-5/H-11	C-8	H-9	101.65
9	4.93	H-11	C-9	C-8/C-10	55.10
10				H-11/H-8	144.55
11	7.16	H-9	C-11	C-12/C-13	126.35
12	7.16	H-11/H-13	C-12	C-13/C-11	126.35
13	7.16	H-12	C-13	C-12/C-11	126.35
14	8.91	H-9		C-1/C-9	

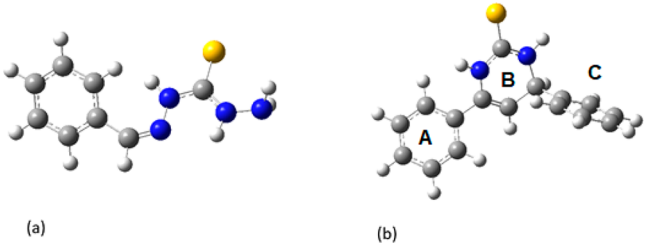

Figure 9. Lowest in energy conformations derived from DFT calculations for (a) **DKI5** and (b) **KKII5**.

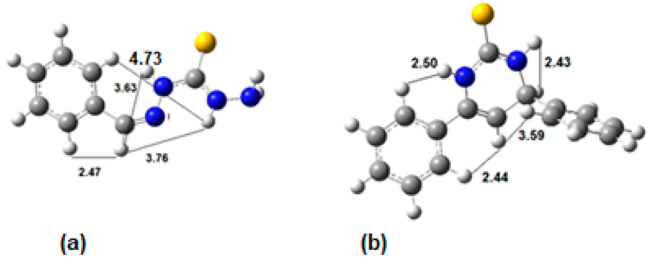

Figure 10. Correlations that were observed in 2D-NOESYs for (a) **DKI5** and (b) **KKII5**.

https://doi.org/10.1021/acsomega.2c07625
ACS Omega 2023, 8, 11966−11977

potential of the LOX-1 active center with the two binding molecules was calculated.

Charges on iron were calculated with Mulliken and NBO analyses. Both predict the same charges (see Table 3). DFT

Table 3. Charges on Fe and Redox Potential for Binding DKI5 and KKII5

DKI5	Mulliken	NBO	$E_{ea}(Fe^{3+} \rightarrow Fe^{2+}) = -\Delta E(attach)$
Fe^{3+}	2.05	2.09	9.6 eV
Fe^{2+}	1.47	1.43	
KKII5	Mulliken	NBO	$E_{ea}(Fe^{3+} \rightarrow Fe^{2+}) = -\Delta E(attach)$
Fe^{3+}	1.32	1.32	6.8 eV
Fe^{2+}	1.41	1.21	

calculations showed that **KKII5** interacts strongly with the amino acids in the active center since it forms smaller bond distances than **DKI5**: 1.91 Å for **KKII5** in contrast to 1.95 Å for **DKI5**. A result of the stronger (shorter) bonds there is an enhanced charge transfer from **KKII5** to Fe^{3+} compared to that with **DKI5**. Note that about 0.9 electrons are transferred from ligands to Fe^{3+} when **DKI5** is binding, while 1.7 electrons are transferred from ligands to Fe^{3+} when **KKII5** is binding. On the contrary, similar charge transfer occurred from ligands to Fe^{2+}, i.e., 0.6 e^- (**DKI5**) and 0.8 e^- (**KKII5**). It is interesting that the binding of the molecules significantly affects the redox potential of the active center of LOX-1. The energy gain for the electron attachment when **KKII5** is binding is significantly smaller by 2.8 eV than that when **DKI5** is binding. This means that **KKII5** enhances the ability of Fe^{3+} to receive electrons compared to **DKI5**; i.e., the active center is further stabilized. This is related to the strong binding interaction of **KKII5** to LOX-1.

In Vitro Biological Assays. Soybean isozyme LOX-1 was used in our in vitro experiments that reveals homology to mammalian lipoxygenase.[40,41] This enzyme uses free fatty acids as substrates[42] and presents maximal activity at pH 9.0. This is achieved by producing a conjugated diene absorbing at 234 nm attributed the conversion of linoleic acid into to 13-hydroperoxylinoleic acid.[43] Both tested biologically compounds present moderate inhibitory activity against the enzyme of LOX-1. The obtained results were compared with the reference compound nor-dihydroguaeretic acid (NDGA) (Table 4). The calculated IC_{50} values of both compounds are

Table 4. In Vitro Inhibition of LOX as IC_{50} Values and % Inhibition of Lipid Peroxidation (%ILP) at 100 μM

code	LOX IC_{50} (μM)	% ILP
DKI5	22.5	94
KKII5	19	98
NDGA	0.45	
Trolox		92

lower in comparison to those of the compound NDGA. Thus, both compounds appear to act as less potent inhibitors. LOXs contain a "non-heme" iron per molecule in the enzyme active site. Iron has a high-spin Fe^{2+} in the native state and high-spin Fe^{3+} in the activated state. A relationship between LOX inhibition and the ability of the inhibitors to reduce Fe^{3+} at the active site to the catalytically inactive Fe^{2+} has been suggested by some studies. This inhibition is related to their ability to reduce the iron species in the active site to the catalytically inactive ferrous form. Furthermore, several LOX inhibitors have been found to be excellent ligands for Fe^{3+}.[44]

2,2-Azobis(2-amidinopropane) hydrochloride AAPH, a water-soluble azo compound, was utilized as a free radical initiator to follow oxidative changes of linoleic acid to conjugated diene hydroperoxide. In the AAPH assay, the highly reactive alkylperoxyl radicals are intercepted mainly by a hydrogen atom transfer (HAT) from the antioxidant.[45] Effective HAT agents are compounds with high hydrogen atom donating ability. More specifically, these are molecules that show low heteroatom−H bond dissociation energies or molecules from which hydrogen abstraction leads to sterically hindered radicals as well as molecules from which abstraction of hydrogen leads to C-centered radicals stabilized by resonance. We compared the antilipid peroxidation activities of both compounds in vitro in comparison to a well-known antioxidant, i.e., Trolox (Table 4). The experimental conditions resemble cellular lipid peroxidation due to the activity of the undertaken radicals. Both tested compounds present high antilipid peroxidation activity compared to the reference compound Trolox. It appears that LOX inhibition is related with the antilipid peroxidation activity. Lipophilicity does not appear to affect the antioxidant activity.

Both compounds significantly inhibit LOX. Between them, **KKII5** was more potent followed by **DKI5**. The higher lipophilicity of **KKII5** compared to that of **DKI5** led to higher inhibitory activity. The reported literature confirms the positive role of lipophilicity for LOX inhibitors.[46]

The majority of the literature records that LOX inhibitors are antioxidants, inhibitors of lipid peroxidation, or free radical scavengers.[46]

EXPERIMENTAL SECTION

General. The reagents are of highest purity from Aldrich, Fluka, and Acros, greater than 98%. Thin layer chromatography was performed on 0.25 mm silica gel plates (E. Merck silica gel 60F254), and the plates were UV visualized. NMR spectra were recorded on a Bruker 400 Avance instrument. A MSQ 400 Surveyor Finnigan instrument was used for mass spectra.

Induced Fit Docking. Induced fit docking has been performed to discover the possible binding of the two molecules (**DKI5** and **KKII5**) in the active site of LOX-1. This enzyme has been selected as a possible target since chalcone and thiocarbohydrazone substructures could serve as potent inhibitors of the enzyme, according to our bibliographic research.[47,48] Furthermore, the Swiss Target webtool (http://www.swisstargetprediction.ch/) revealed LOX as a potent target for both two molecules. The crystal structure used for the in silico studies was PDB ID 5T5V.[49] The in silico calculations were performed using protein preparation wizard module available in Schrödinger Suites to prepare the crystal structure. Since LOX is a metalloprotein, several computational challenges had be addressed. Thus, the quantum effects associated with the presence of an Fe^{3+} cation in LOX's active site were determined with the "create zero-order bonds to metals" module of the Schrödinger's Maestro molecular modeling platform. In this module, the bonds to metals are broken and new zero-order bonds between metals and nearby atoms are added. Furthermore, the formal charges are corrected to constrain the X-ray acquired coordination geometry.

https://doi.org/10.1021/acsomega.2c07625
ACS Omega 2023, 8, 11966−11977

The two compounds were sketched in Schrödinger's Maestro[50] molecular modeling platform and minimized using Macromodel[51] and DFT calculations. LigPrep was used to prepare the 3D models, taking into account their stereochemistry features. During the ligand preparation, the "add metal binding states" option of the Epik module of LigPrep was chosen. If this option was not selected, the binding would fail as it would be characterized by high energy state penalties. The geometries were optimized with MacroModel and during the structure relxation process chiral centers were checked that retained their proper chiralities. The force field OPLS2005[52] was used for minimization and proper treatment of their protonation states at physiological pH (∼7.4). Hammett and Taft methods have been implemented in conjunction with an ionization tool to generate chemically sensible 3D models. Ligand structures were furthermore rigorously minimized by MacroModel with water as the solvent and OPLS2005 as the force field, using a conjugate gradient (CG) method with a threshold of 0.01 kcal/mol. The derived minimized structures were used as input to a mixed-torsional/low-sampling conformational search forced to avoid the modification of the input chiralities. Conformational search generated several conformers for each molecule that were energetically ranked. The most favored conformation was used as input for the docking calculations.

The calculations were performed using the induced fit docking (IFD) method available in Schrödinger Suites. The ligand was docked in the 5 energetically favored conformations generated by Macromodel. Prior to the free binding calculations, protein preparation constrained refinement was applied in the Glide docking stage. Trimming side chains automatically (based on B-factor) and Prime refinement of the protein side chains were applied, and the docking process was accomplished by Glide/XP. During the docking process, the dielectric constant of the active site was set to 80 and the waters in the crystallographic data were preserved.

Molecular Dynamics. The MD simulation system was set up with SPC/E modeled waters surrounding the drug−protein complex and neutralized with Na^+ and Cl^- ions until the experimental salt concentration of 0.150 M NaCl was reached. The N-terminus of the protein was capped by an acetyl group, whereas the C-terminus remained uncapped since it is part of the protein's active site. The OPLS2005 force field was used to model all protein−ligand interactions, and the long-range electrostatics were treated with the particle mesh Ewald method (PME)[53,54] and a grid spacing of 0.8 Å. van der Waals and short-range electrostatic interactions were smoothly truncated at 9.0 Å. During the calculations, the temperature was kept constant using the Nosé−Hoover thermostat,[55] while the Martyna−Tobias−Klein method[54] was used to control the pressure. Calculations were performed using periodic conditions and a simulation box with dimensions of 10.0 × 10.0 × 10.0 A. The equations of motion were integrated using the multistep RESPA integrator[56] with an inner time step of 2 fs for bonded interactions and nonbonded interactions within a cutoff of 9 Å. An outer time step of 6.0 fs was used for nonbonded interactions beyond the cutoff. Each system was equilibrated using the default protocol provided by Desmond.[57] The system was relaxed initially with Brownian dynamics simulation in the NVT ensemble at T = 310 K with restraints on solute heavy atoms. Before starting with the production phase, the system was left to relax in the NPT ensemble with no restraints for 1.0 ns. The production phase of the MD simulation was set to 200 ns. This time is sufficient to obtain adequate sample size to analyze the complexing of the drug in the enzyme active site cavity.

The MD simulations were run in workstations using the GPU implementation of the MD simulations codes and the statistics of simulation were evaluated based on the RMSD convergence of the protein backbone Cα atoms and the RMSD of the ligand.

All MD simulations were performed three times to verify the reproducibility of the results, and the trajectory was analyzed with the Desmond and VMD trajectory analysis tools.

MM/GBSA Calculations. MM/GBSA was used to determine free binding energy of the complexes of the two molecules with their target proteins. Specifically, the most favored interactions contributing more to the formation of the complexes were calculated using the Prime module of Maestro. In particular, the MM/GBSA calculations were applied to three most favored energetically ligand−protein complexes extracted from MD trajectory cluster analysis. VSGB solvation was used to describe protein flexibility.[58]

Synthesis. *(E)-N′-Benzylidenehydrazinecarbothiohydrazide,* ***DKI5****.*[59]

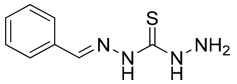

To a stirred solution of benzaldehyde (0.14 mL, 1.4 mmol) in ethanol 70% (90 mL) was added thiocarbohydrazide (0.29 g, 2.8 mmol) followed by the addition of 1 drop of acetic acid. The reaction mixture was heated to 80 °C for 4 h. Then the reaction mixture was left to stand at room temperature, filtered, washed with ethanol/water 1:1, and recrystallized from ethanol to give **DKI5** as an off-white solid in 75% yield. R_f (PE/EtOAc: 2/1) = 0.73.

4,6-Diphenyl-3,4-dihydropyrimidine-2(1H)-thione, ***KKII5****.*[60]

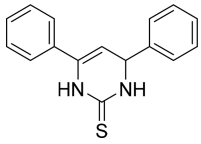

To a stirred solution of NaOH (68 mg, 1.70 mmol) in EtOH (3.5 mL) were added *E*-chalcone (0.35 g, 1.70 mmol) and thiourea (0.13 g, 1.70 mmol), and the mixture was sonicated for 1 h at room temperature. Then it was poured in ice−water, and the solid formed was filtered, washed with H_2O, EtOH/H_2O 1:1, and dried to give **KKII5** as an off-yellow solid in 97% yield. R_f (PE/AcOEt 9.5/0.5) = 0.71.

Structure Assignment. The two molecules have been identified using a 400 MHz NMR Bruker Avance spectrometer operated at 25 °C. The pulse sequences used were obtained from the library of the spectrometer. Data processing including sinebell apodization, Fourier transformation, phasing symmetrization, and plotting were performed using TopSpin Bruker Data Analysis and MestreNova[61] software packages.

Quantum Mechanics Calculations: DFT Calculations. Conformational analysis of the **DKI5** and **KKII5** molecules was performed employing DFT[62] at the B3LYP[63,64]/6-311+G(d,p)[65] level of theory. All compounds were optimized to find the lowest minima. All calculations were performed using DMSO solvent employing the polarizable continuum model (PCM).[66−68]

https://doi.org/10.1021/acsomega.2c07625
ACS Omega 2023, 8, 11966−11977

Furthermore, the binding of **DKI5** and **KKII5** in the active site of LOX-1 was calculated via DFT(B3LYP/6-311+G(d,p)) methodology. The geometries of the LOX-1 active center with the binding molecules, obtained via MD calculations, were used as the initial guess for the DFT calculations. The complexes included about 200 atoms, and they were geometry optimized considering iron is complexed with two oxidation states +2 and +3 to check the effect of the oxidation state on the binding, the electron transfer, and the redox potential of LOX-1. The charges of the iron center and ligands were calculated using two population analyses, i.e., Mulliken and NBO.[69] Calculations and visualization were carried out via Gaussian 16.[70]

In Vitro Studies. UV−vis spectra, for the in vitro tests, were obtained on a Shimadzu 1700Spec UV double-beam spectrophotometer (PerkinElmer Corporation Ltd., Lane Beaconsfield, Bucks, UK). Soybean lipoxygenase, sodium linoleate, and 2,2-azobis(2-amidinopropane)dihydrochloride (AAPH) were purchased from Sigma Chemical, Co. (St. Louis, MO, USA).

The in vitro assays were performed at a concentration of 100 μM (a 10 mMstock solution in DMSO was used, from which several dilutions were made). The IC_{50} values of the samples studied were calculated using at least triplicates, and the standard deviation of absorbance did not exceed 10% of the mean. The compounds prior to be recorded were diluted in 0.1% DMSO under sonification in an appropriate buffer in several dilutions. Statistical comparisons were made using the Student t test. A statistically significant difference was defined as $p < 0.05$.

Inhibition of Linoleic Acid Peroxidation. In vitro study was performed as described by Hadjipavlou et al.[48] Ten microliters of the 16 mM sodium linoleate solution were added to the UV cuvette containing 0.93 mL of a 0.05 mM phosphate buffer, pH 7.4, and prethermostated at 37 °C. Addition of 50 μL of a 40 mM free radical initiator AAPH solution initiated at 37 °C the oxidation reaction. Oxidation was monitored at 234 nm and was performed in the presence of aliquots (10 μL) without the use of antioxidants. Lipid oxidation was achieved and recorded in the presence of the same level of DMSO which served as a negative control. Trolox was used as the appropriate standard (positive control).

Soybean Lipoxygenase Inhibition Study. The in vitro study was performed as described by Hadjipavlou-Litina et al.[48] The compounds were incubated at room temperature with sodium linoleate (0.1 mM) and 0.2 mL of enzyme solution ($1/9.10^{-4}$ w/v in saline), and the conversion of sodium linoleate to 13-hydroperoxylinoleic acid at 234 nm was calculated quantitatively. Nor-dihydroguaeretic acid NDGA (IC_{50} = 0.45 μM) was used as a standard (positive control). To determine their IC_{50} values we have used six ascending concentrations (0.01−100 μM). To assess the repeatability and accuracy of the experiments they were repeated with the same experimental conditions in six duplicate replicates. The calculated results are reported from the mean of the six experiments. It was found that the standard deviation was less than 10% (a = 0.01). Prior to the experiments, a blank determination was used as a negative control.

CONCLUSIONS

Two thiosemicarbazone analogues, the 4,6-diphenyl-3,4-dihydropyrimidine-2(1*H*)-thione (**KKII5**) and (*E*)-*N*′-benzylidenehydrazinecarbothiohydrazide (**DKI5**), were synthesized here in high yield up to 97% using known methodology. Their unambiguous structures were studied utilizing 1D and 2D homonuclear and heteronuclear NMR, 2D-NOESY, and DFT methodology.

The low energy conformers of the two compounds have been used for molecular docking experiments in LOX-1 enzyme. The promising favored binding energies of both molecules triggered our interest to evaluate them with an in vitro test. MD simulations showed that both molecules are stabilized in their binding cavity. The experimental results were also promising, showing that both compounds have considerable inhibitory activity (IC_{50} was 22.5 μM for **DKI5** and 19.5 μM for **KKII5**).

The redox potential of the active center of LOX-1 with the binding molecule was calculated via DFT methodology. It is interestingly found that the energy gain for the electron attachment in the active center of LOX-1 is significantly smaller when **KKII5** is binding than when **DKI5** is binding, by about 3 eV, meaning that **KKII5** enhanced importantly the ability of the active center to receive electrons comparing to **DKI5**. This is related to the strong binding interaction of **KKII5** to LOX.

Finally, our ADMET studies showed that the two molecules lack of considerable toxicity and can be used for future studies as drug leads.

ASSOCIATED CONTENT

Supporting Information

The Supporting Information is available free of charge at https://pubs.acs.org/doi/10.1021/acsomega.2c07625.

2D-NOESY-NMR spectra of DKI5, 2D-NOESY-NMR spectra of KKII5, 2D HSQC $^{15}N-^{1}H$ spectra of KKII5, and structure assignment of DKI5 (Figure S1); spectra were recorded in DMSO-d_6 on a Bruker AC 400 MHz spectrometer at 25 °C; ^{13}C NMR spectra of DKI5, ^{13}C spectra of KKII5, 2D-HMBC $^{15}N-^{1}H$ spectra of DKI5, and structure assignment of KKII5 (Figure S2); spectra were recorded in DMSO-d_6 on a Bruker AC 400 MHz spectrometer at 25 °C; 2D-HSQC-NMR spectra of DKI5, 2D-HSQC spectra of KKII5, and 2D-HSQC $^{15}N-^{1}H$ spectra of DKI5 (Figure S3); spectra were recorded in DMSO-d_6 on a Bruker AC 400 MHz spectrometer at 25 °C; 2D-HMBC-NMR spectra of DKI5 and 2D-HMBC spectra of KKII5 (Figure S4); spectra were recorded in DMSO-d_6 on a Bruker AC 400 MHz spectrometer at 25 °C (PDF)

AUTHOR INFORMATION

Corresponding Authors

Demeter Tzeli − *Laboratory of Physical Chemistry, Department of Chemistry, National and Kapodistrian University of Athens, 11571 Athens, Greece; Theoretical and Physical Chemistry Institute, National Hellenic Research Foundation, 11635 Athens, Greece;* orcid.org/0000-0003-0899-7282; Email: tzeli@chem.uoa.gr

Stamatia Vassiliou − *Laboratory of Organic Chemistry, Department of Chemistry, National and Kapodistrian University of Athens, 11571 Athens, Greece;* Email: svassiliou@chem.uoa.gr

Thomas Mavromoustakos − *Laboratory of Organic Chemistry, Department of Chemistry, National and*

https://doi.org/10.1021/acsomega.2c07625
ACS Omega 2023, 8, 11966−11977

Kapodistrian University of Athens, 11571 Athens, Greece; Email: tmavrom@chem.uoa.gr

Authors

Nikitas Georgiou − *Laboratory of Organic Chemistry, Department of Chemistry, National and Kapodistrian University of Athens, 11571 Athens, Greece*; orcid.org/0000-0002-3226-7434

Eleni Chontzopoulou − *Laboratory of Organic Chemistry, Department of Chemistry, National and Kapodistrian University of Athens, 11571 Athens, Greece*

Antigoni Cheilari − *Department of Pharmacognosy and Natural Products Chemistry, Faculty of Pharmacy, National and Kapodistrian University of Athens, 15771 Athens, Greece*

Aikaterini Katsogiannou − *Laboratory of Organic Chemistry, Department of Chemistry, National and Kapodistrian University of Athens, 11571 Athens, Greece*

Danai Karta − *Laboratory of Organic Chemistry, Department of Chemistry, National and Kapodistrian University of Athens, 11571 Athens, Greece*

Kyriaki Vavougyiou − *Laboratory of Organic Chemistry, Department of Chemistry, National and Kapodistrian University of Athens, 11571 Athens, Greece*

Dimitra Hadjipavlou-Litina − *Department of Pharmaceutical Chemistry, School of Pharmacy, Faculty of Health Sciences, Aristotle University of Thessaloniki, 54124 Thessaloniki, Greece*

Uroš Javornik − *Slovenian NMR Centre, National Institute of Chemistry, SI-1001 Ljubljana, Slovenia*

Janez Plavec − *Slovenian NMR Centre, National Institute of Chemistry, SI-1001 Ljubljana, Slovenia*; orcid.org/0000-0003-1570-8602

Complete contact information is available at: https://pubs.acs.org/10.1021/acsomega.2c07625

Notes

The authors declare no competing financial interest.

■ ACKNOWLEDGMENTS

The authors acknowledge the CERIC−ERIC consortium for the access to experimental facilities and financial support. Materials were supported by Special Account for Research Grants (SARG), National Kapodistrian University of Athens (NKUA). U.J. and J.P. acknowledge financial support of Slovenian Research Agency (ARRS, Grant P1-242).

■ REFERENCES

(1) Othman, E. M.; Fayed, E. A.; Husseiny, E. M.; Abulkhair, H. S. Rationale Design, Synthesis, Cytotoxicity Evaluation, and in Silico Mechanistic Studies of Novel 1,2,3-Triazoles with Potential Anticancer Activity. *New J. Chem.* **2022**, *46* (25), 12206−12216.

(2) Othman, E. M.; Fayed, E. A.; Husseiny, E. M.; Abulkhair, H. S. The Effect of Novel Synthetic Semicarbazone- and Thiosemicarbazone-Linked 1,2,3-Triazoles on the Apoptotic Markers, VEGFR-2, and Cell Cycle of Myeloid Leukemia. *Bioorg. Chem.* **2022**, *127*, 105968.

(3) Ouyang, Y.; Li, J.; Chen, X.; Fu, X.; Sun, S.; Wu, Q. Chalcone Derivatives: Role in Anticancer Therapy. *Biomolecules* **2021**, *11* (6), 894.

(4) Dan, W.; Dai, J. Recent Developments of Chalcones as Potential Antibacterial Agents in Medicinal Chemistry. *Eur. J. Med. Chem.* **2020**, *187*, 111980.

(5) Zhou, Q.; Tang, X.; Chen, S.; Zhan, W.; Hu, D.; Zhou, R.; Sun, N.; Wu, Y.; Xue, W. Design, Synthesis, and Antifungal Activity of Novel Chalcone Derivatives Containing a Piperazine Fragment. *J. Agric. Food Chem.* **2022**, *70* (4), 1029−1036.

(6) Qin, H.-L.; Zhang, Z.-W.; Lekkala, R.; Alsulami, H.; Rakesh, K. P. Chalcone Hybrids as Privileged Scaffolds in Antimalarial Drug Discovery: A Key Review. *Eur. J. Med. Chem.* **2020**, *193*, 112215.

(7) Kaushal, R.; Kaur, M. Bio-Medical Potential of Chalcone Derivatives and Their Metal Complexes as Antidiabetic Agents: A Review. *J. Coord. Chem.* **2021**, *74* (4−6), 725−742.

(8) Nowakowska, Z. A Review of Anti-Infective and Anti-Inflammatory Chalcones. *Eur. J. Med. Chem.* **2007**, *42* (2), 125−137.

(9) Sogawa, S.; Nihro, Y.; Ueda, H.; Izumi, A.; Miki, T.; Matsumoto, H.; Satoh, T. 3,4-Dihydroxychalcones as Potent 5-Lipoxygenase and Cyclooxygenase Inhibitors. *J. Med. Chem.* **1993**, *36* (24), 3904−3909.

(10) Zeraik, M. L.; Pauli, I.; Dutra, L. A.; Cruz, R. S.; Valli, M.; Paracatu, L. C.; de Faria, C. M. Q. G.; Ximenes, V. F.; Regasini, L. O.; Andricopulo, A. D.; Bolzani, V. S. Identification of a Prenyl Chalcone as a Competitive Lipoxygenase Inhibitor: Screening, Biochemical Evaluation and Molecular Modeling Studies. *Molecules* **2021**, *26* (8), 2205.

(11) Okolo, E. N.; Ugwu, D. I.; Ezema, B. E.; Ndefo, J. C.; Eze, F. U.; Ezema, C. G.; Ezugwu, J. A.; Ujam, O. T. New Chalcone Derivatives as Potential Antimicrobial and Antioxidant Agent. *Sci. Rep.* **2021**, *11* (1), 21781.

(12) K. Sahu, N.; S. Balbhadra, S.; Choudhary, J.; V. Kohli, D. Exploring Pharmacological Significance of Chalcone Scaffold: A Review. *Curr. Med. Chem.* **2012**, *19* (2), 209−225.

(13) Higuchi, K.; Watanabe, T.; Tanigawa, T.; Tominaga, K.; Fujiwara, Y.; Arakawa, T. Sofalcone, a Gastroprotective Drug, Promotes Gastric Ulcer Healing Following Eradication Therapy for Helicobacter Pylori: A Randomized Controlled Comparative Trial with Cimetidine, an H2-Receptor Antagonist. *J. Gastroenterol. Hepatol.* **2010**, *25*, S155−S160.

(14) Cho, S.; Kim, S.; Jin, Z.; Yang, H.; Han, D.; Baek, N.-I.; Jo, J.; Cho, C.-W.; Park, J.-H.; Shimizu, M.; Jin, Y.-H. Isoliquiritigenin, a Chalcone Compound, Is a Positive Allosteric Modulator of GABAA Receptors and Shows Hypnotic Effects. *Biochem. Biophys. Res. Commun.* **2011**, *413* (4), 637−642.

(15) Langley, B. O.; Ryan, J. J.; Hanes, D.; Phipps, J.; Stack, E.; Metz, T. O.; Stevens, J. F.; Bradley, R. Xanthohumol Microbiome and Signature in Healthy Adults (the XMaS Trial): Safety and Tolerability Results of a Phase I Triple-Masked, Placebo-Controlled Clinical Trial. *Mol. Nutr. Food Res.* **2021**, *65* (8), 2001170.

(16) Parhiz, H.; Roohbakhsh, A.; Soltani, F.; Rezaee, R.; Iranshahi, M. Antioxidant and Anti-Inflammatory Properties of the Citrus Flavonoids Hesperidin and Hesperetin: An Updated Review of Their Molecular Mechanisms and Experimental Models. *Phyther. Res.* **2015**, *29* (3), 323−331.

(17) Fayed, E. A.; Mohsen, M.; El-Gilil, S. M. A.; Aboul-Magd, D. S.; Ragab, A. Novel Cyclohepta[b]Thiophene Derivative Incorporating Pyrimidine, Pyridine, and Chromene Moiety as Potential Antimicrobial Agents Targeting DNA Gyrase. *J. Mol. Struct.* **2022**, *1262*, 133028.

(18) Kurzer, F.; Wilkinson, M. Chemistry of Carbohydrazide and Thiocarbohydrazide. *Chem. Rev.* **1970**, *70* (1), 111−149.

(19) Kadam, S. S.; Gotarne, R. P.; Shinde, M. N.; Mane, V. S.; Khan, A. A.; Kumbhar, A. A. Fe(III), Co(II), Ni(II), Cu(II) and Zn(II) Complexes of Fluorophore-Anchored Asymmetric Thiocarbohydrazone: Synthesis, Characterization and Biological Studies. *Inorg. Chim. Acta* **2022**, *536*, 120887.

(20) Makarieva, T. N.; Tabakmaher, K. M.; Guzii, A. G.; Denisenko, V. A.; Dmitrenok, P. S.; Shubina, L. K.; Kuzmich, A. S.; Lee, H.-S.; Stonik, V. A. Monanchocidins B-E: Polycyclic Guanidine Alkaloids with Potent Antileukemic Activities from the Sponge Monanchora Pulchra. *J. Nat. Prod.* **2011**, *74* (9), 1952−1958.

(21) Boukis, A. C.; Llevot, A.; Meier, M. A. R. High Glass Transition Temperature Renewable Polymers via Biginelli Multicomponent Polymerization. *Macromol. Rapid Commun.* **2016**, *37* (7), 643−649.

(22) Zhao, Y.; Yu, Y.; Zhang, Y.; Wang, X.; Yang, B.; Zhang, Y.; Zhang, Q.; Fu, C.; Wei, Y.; Tao, L. From Drug to Adhesive: A New

Application of Poly(Dihydropyrimidin-2(1H)-One)s via the Biginelli Polycondensation. *Polym. Chem.* **2015**, *6* (27), 4940−4945.
(23) Desta, D.; Sjoholm, R.; Lee, L.; Lee, M.; Dittenhafer, K.; Canche, S.; Babu, B.; Chavda, S.; Dewar, C.; Yanow, S.; Best, A. A.; Lee, M. Synthesis and Antiprotozoal Activity of 1,2,3,4-Tetrahydro-2-Thioxopyrimidine Analogs of Combretastatin A-4. *Med. Chem. Res.* **2011**, *20* (3), 364−369.
(24) El-Meligie, S.; Taher, A. T.; Kamal, A. M.; Youssef, A. Design, Synthesis and Cytotoxic Activity of Certain Novel Chalcone Analogous Compounds. *Eur. J. Med. Chem.* **2017**, *126*, 52−60.
(25) Lee, L.; Davis, R.; Vanderham, J.; Hills, P.; Mackay, H.; Brown, T.; Mooberry, S. L.; Lee, M. 1,2,3,4-Tetrahydro-2-Thioxopyrimidine Analogs of Combretastatin-A4. *Eur. J. Med. Chem.* **2008**, *43* (9), 2011−2015.
(26) Fayed, E. A.; Nosseir, E. S.; Atef, A.; El-Kalyoubi, S. A. In Vitro Antimicrobial Evaluation and in Silico Studies of Coumarin Derivatives Tagged with Pyrano-Pyridine and Pyrano-Pyrimidine Moieties as DNA Gyrase Inhibitors. *Mol. Divers.* **2022**, *26* (1), 341−363.
(27) Fayed, E. A.; Bayoumi, A. H.; Saleh, A. S.; Ezz Al-Arab, E. M.; Ammar, Y. A. In Vivo and in Vitro Anti-Inflammatory, Antipyretic and Ulcerogenic Activities of Pyridone and Chromenopyridone Derivatives, Physicochemical and Pharmacokinetic Studies. *Bioorg. Chem.* **2021**, *109*, 104742.
(28) Pisoschi, A. M.; Pop, A.; Iordache, F.; Stanca, L.; Geicu, O. I.; Bilteanu, L.; Serban, A. I. Antioxidant, Anti-Inflammatory and Immunomodulatory Roles of Vitamins in COVID-19 Therapy. *Eur. J. Med. Chem.* **2022**, *232*, 114175.
(29) Fayed, E. A.; Al-Arab, E. M. E.; Saleh, A. S.; Bayoumi, A. H.; Ammar, Y. A. Design, Synthesis, in Silico Studies, in Vivo and in Vitro Assessment of Pyridones and Thiazolidinones as Anti-Inflammatory, Antipyretic and Ulcerogenic Hits. *J. Mol. Struct.* **2022**, *1260*, 132839.
(30) Brash, A. R. Lipoxygenases: Occurrence, Functions, Catalysis, and Acquisition of Substrate. *J. Biol. Chem.* **1999**, *274* (34), 23679−23682.
(31) Yamamoto, S. Mammalian Lipoxygenases: Molecular Structures and Functions. *Biochim. Biophys. Acta - Lipids Lipid Metab.* **1992**, *1128* (2−3), 117−131.
(32) Feltenmark, S.; Gautam, N.; Brunnstrom, A.; Griffiths, W.; Backman, L.; Edenius, C.; Lindbom, L.; Bjorkholm, M.; Claesson, H.-E. Eoxins Are Proinflammatory Arachidonic Acid Metabolites Produced via the 15-Lipoxygenase-1 Pathway in Human Eosinophils and Mast Cells. *Proc. Natl. Acad. Sci. U. S. A.* **2008**, *105* (2), 680−685.
(33) Alavi, S. J.; Sadeghian, H.; Seyedi, S. M.; Salimi, A.; Eshghi, H. A Novel Class of Human 15-LOX-1 Inhibitors Based on 3-Hydroxycoumarin. *Chem. Biol. Drug Des.* **2018**, *91* (6), 1125−1132.
(34) Daina, A.; Michielin, O.; Zoete, V. SwissADME: A Free Web Tool to Evaluate Pharmacokinetics, Drug-Likeness and Medicinal Chemistry Friendliness of Small Molecules. *Sci. Rep.* **2017**, *7*, 42717.
(35) Pires, D. E. V.; Blundell, T. L.; Ascher, D. B. PkCSM: Predicting Small-Molecule Pharmacokinetic and Toxicity Properties Using Graph-Based Signatures. *J. Med. Chem.* **2015**, *58* (9), 4066−4072.
(36) Viana Nunes, A. M.; das Chagas Pereira de Andrade, F.; Filgueiras, L. A.; de Carvalho Maia, O. A.; Cunha, R. L. O. R.; Rodezno, S. V. A.; Maia Filho, A. L. M.; de Amorim Carvalho, F. A.; Braz, D. C.; Mendes, A. N. PreADMET Analysis and Clinical Aspects of Dogs Treated with the Organotellurium Compound RF07: A Possible Control for Canine Visceral Leishmaniasis? *Environ. Toxicol. Pharmacol.* **2020**, *80*, 103470.
(37) Matsoukas, J.M.; Hondrelis, J.; Keramida, M.; Mavromoustakos, T.; Makriyannis, A.; Yamdagni, R.; Wu, Q.; Moore, G.J. Role of the NH2-Terminal Domain of Angiotensin [SarllAngiotensin I1 on Conformation and Activity. *Biochemistry* **1994**, *269*, 5303.
(38) Preto, M. A. C.; Melo, A.; Maia, H. L. S.; Mavromoustakos, T.; Ramos, M. J. Molecular Dynamics Simulations of Angiotensin II in Aqueous and Dimethyl Sulfoxide Environments. *J. Phys. Chem. B* **2005**, *109* (37), 17743−17751.
(39) Besse, P.; Combourieu, B.; Boyse, G.; Sancelme, M.; De Wever, H.; Delort, A. M. Long-Range 1H-15N Heteronuclear Shift Correlation at Natural Abundance: A Tool to Study Benzothiazole Biodegradation by Two Rhodococcus Strains. *Appl. Environ. Microbiol.* **2001**, *67* (4), 1412−1417.
(40) Minor, W.; Steczko, J.; Bolin, J. T.; Otwinowski, Z.; Axelrod, B. Crystallographic Determination of the Active Site Iron and Its Ligands in Soybean Lipoxygenase L-1. *Biochemistry* **1993**, *32* (25), 6320−6323.
(41) Skrzypczak-Jankun, E.; Amzel, L. M.; Kroa, B. A.; Funk, M.O. Structure of Soybean Lipoxygenase L3 and a Comparison with Its L1 Isoenzyme. *Proteins* **1997**, *29* (1), 15−31.
(42) Moody, T. W.; Leyton, J.; Martinez, A.; Hong, S.; Malkinson, A.; Mulshine, J. L. Lipoxygenase Inhibitors Prevent Lung Carcinogenesis and Inhibit Non-Small Cell Lung Cancer Growth. *Exp. Lung Res.* **1998**, *24* (4), 617−628.
(43) Maccarrone, M.; van Aarle, P. G.; Veldink, G. A.; Vliegenthart, J. F. In Vitro Oxygenation of Soybean Biomembranes by Lipoxygenase-2. *Biochim. Biophys. Acta - Biomembr.* **1994**, *1190* (1), 164−169.
(44) Boukamp, P.; Petrussevska, R. T.; Breitkreutz, D.; Hornung, J.; Markham, A.; Fusenig, N. E. Normal Keratinization in a Spontaneously Immortalized Aneuploid Human Keratinocyte Cell Line. *J. Cell Biol.* **1988**, *106* (3), 761−771.
(45) Huang, D.; Ou, B.; Prior, R. L. The Chemistry behind Antioxidant Capacity Assays. *J. Agric. Food Chem.* **2005**, *53* (6), 1841−1856.
(46) Pontiki, E.; Hadjipavlou-Litina, D. Lipoxygenase Inhibitors: A Comparative QSAR Study Review and Evaluation of New QSARs. *Med. Res. Rev.* **2008**, *28* (1), 39−117.
(47) Ghafary, S.; Ghobadian, R.; Mahdavi, M.; Nadri, H.; Moradi, A.; Akbarzadeh, T.; Najafi, Z.; Sharifzadeh, M.; Edraki, N.; Moghadam, F. H.; Amini, M. Design, Synthesis, and Evaluation of Novel Cinnamic Acid-Tryptamine Hybrid for Inhibition of Acetylcholinesterase and Butyrylcholinesterase. *DARU J. Pharm. Sci.* **2020**, *28* (2), 463−477.
(48) Peperidou, A.; Pontiki, E.; Hadjipavlou-Litina, D.; Voulgari, E.; Avgoustakis, K. Multifunctional Cinnamic Acid Derivatives. *Molecules* **2017**, *22* (8), 1247.
(49) Offenbacher, A. R.; Hu, S.; Poss, E. M.; Carr, C. A. M.; Scouras, A. D.; Prigozhin, D. M.; Iavarone, A. T.; Palla, A.; Alber, T.; Fraser, J. S.; Klinman, J. P. Hydrogen-Deuterium Exchange of Lipoxygenase Uncovers a Relationship between Distal, Solvent Exposed Protein Motions and the Thermal Activation Barrier for Catalytic Proton-Coupled Electron Tunneling. *ACS Cent. Sci.* **2017**, *3* (6), 570−579.
(50) *L.L.C. MacroModel*, version 10; Schrödinger: New York, 2013.
(51) *L.L.C. MacroModel*, version 10.2; Schrödinger: New York, 2013.
(52) Jorgensen, W. L.; Maxwell, D. S.; Tirado-Rives, J. Development and Testing of the OPLS All-Atom Force Field on Conformational Energetics and Properties of Organic Liquids. *J. Am. Chem. Soc.* **1996**, *118* (45), 11225−11236.
(53) Essmann, U.; Perera, L.; Berkowitz, M. L.; Darden, T.; Lee, H.; Pedersen, L. G. A Smooth Particle Mesh Ewald Method. *J. Chem. Phys.* **1995**, *103*, 8577.
(54) Martyna, G. J.; Tobias, D. J.; Klein, M. L. Constant Pressure Molecular Dynamics Algorithms. *J. Chem. Phys.* **1994**, *101*, 4177−4189.
(55) Humphreys, D. D.; Friesner, R. A.; Berne, B. J. A Multiple-Time-Step Molecular Dynamics Algorithm for Macromolecules. *J. Phys. Chem.* **1994**, *98*, 6885.
(56) Lyman, E.; Zuckerman, D. M. Ensemble-Based Convergence Analysis of Biomolecular Trajectories. *Biophys. J.* **2006**, *91*, 164−172.
(57) *Desmond Tutorial*, version D.D.; Schrödinger, https://doi.org/doi:10.1162/rest_a_00790.
(58) Pattar, S. V.; Adhoni, S. A.; Kamanavalli, C. M.; Kumbar, S. S. In Silico Molecular Docking Studies and MM/GBSA Analysis of Coumarin-Carbonodithioate Hybrid Derivatives Divulge the Anticancer Potential against Breast Cancer. *Beni-Suef Univ. J. Basic Appl. Sci.* **2020**, *9* (1), 36.

https://doi.org/10.1021/acsomega.2c07625
ACS Omega 2023, 8, 11966−11977

(59) Li, Z.; Feng, X.; Zhao, Y. Microwave Induced Efficient Synthesis of (Un)Substituted Benzaldehyde (5-Aryl-1,3,4-Thiadiazol-2-Yl)Hydrazones Using Silica-Supported Dichlorophosphate as a Recoverable Dehydrant. *J. Heterocycl. Chem.* **2008**, *45* (5), 1489−1492.
(60) Abbass, S. A.; Moustafa, G. A. I.; Hassan, H. A.; Abuo-Rahma, G. E.-D. A. Facile One-Pot Three-Component Synthesis of 4,6-Diaryl-3,4-Dihydropyrimidine-2(1 H)-Thiones under Ultrasonic Irradiation. *Synth. Commun.* **2019**, 1−6.
(61) Willcott, M. R. MestRe Nova. *J. Am. Chem. Soc.* **2009**, *131* (36), 13180−13180.
(62) Tirado-Rives, J.; Jorgensen, W. L. Performance of B3LYP Density Functional Methods for a Large Set of Organic Molecules. *J. Chem. Theory Comput.* **2008**, *4* (2), 297−306.
(63) Lee, C.; Yang, W.; Parr, R. G. Development of the Colle-Salvetti Correlation-Energy Formula into a Functional of the Electron Density. *Phys. Rev. B* **1988**, *37* (2), 785−789.
(64) Becke, A. D. A New Mixing of Hartree-Fock and Local Density-functional Theories. *J. Chem. Phys.* **1993**, *98* (2), 1372−1377.
(65) Curtiss, L. A.; McGrath, M. P.; Blaudeau, J.; Davis, N. E.; Binning, R. C.; Radom, L. Extension of Gaussian-2 Theory to Molecules Containing Third-row Atoms Ga-Kr. *J. Chem. Phys.* **1995**, *103* (14), 6104−6113.
(66) Miertuš, S.; Scrocco, E.; Tomasi, J. Electrostatic Interaction of a Solute with a Continuum. A Direct Utilizaion of AB Initio Molecular Potentials for the Prevision of Solvent Effects. *Chem. Phys.* **1981**, *55* (1), 117−129.
(67) Tomasi, J.; Mennucci, B.; Cammi, R. Quantum Mechanical Continuum Solvation Models. *Chem. Rev.* **2005**, *105* (8), 2999−3094.
(68) Tzeli, D.; Tsoungas, P. G.; Petsalakis, I. D.; Kozielewicz, P.; Zloh, M. Intramolecular Cyclization of *β*-Nitroso-o-Quinone Methides. A Theoretical Endoscopy of a Potentially Useful Innate 'Reclusive' Reaction. *Tetrahedron* **2015**, *71* (2), 359−369.
(69) Saha, S.; Roy, R. K.; Ayers, P. W. Are the Hirshfeld and Mulliken Population Analysis Schemes Consistent with Chemical Intuition? *Int. J. Quantum Chem.* **2009**, *109* (9), 1790−1806.
(70) Frisch, M. J.; Trucks, G. W.; Schlegel, H. B.; Scuseria, G. E.; Robb, M. A.; Cheeseman, J. R.; Scalmani, G.; Barone, V.; Petersson, G. A.; Nakatsuji, H.; Li, X.; Caricato, M.; Marenich, A. V.; Bloino, J.; Janesko, B. G.; Gomperts, R.; Mennucci, B.; Hratchian, H. P.; et al. *Gaussian 16*, revision B.01; Gaussian Inc.: Wallingford, CT, 2016.

https://doi.org/10.1021/acsomega.2c07625
ACS Omega 2023, 8, 11966−11977